


Behavior of gapped and ungapped Dirac cones in the antiferromagnetic topological metal SmBi

Anup Pradhan Sakhya,¹ Shiv Kumar,² Arindam Pramanik,¹ Ram Prakash Pandeya,¹ Rahul Verma,¹ Bahadur Singh,¹ Sawani Datta,¹ Souvik Sasmal,¹ Rajib Mondal,¹ Eike F. Schwier,² Kenya Shimada,² A. Thamizhavel,¹ and Kalobaran Maiti^{1,*}

¹*Department of Condensed Matter Physics and Materials Science, Tata Institute of Fundamental Research, Homi Bhabha Road, Colaba, Mumbai-400005, India*

²*Hiroshima Synchrotron Radiation Center, Hiroshima University, 2-313 Kagamiyama, Higashi-Hiroshima 739-0046, Japan*

 (Received 4 September 2021; revised 3 February 2022; accepted 12 August 2022; published 23 August 2022)

We studied the behavior of nontrivial Dirac fermion states in the antiferromagnetic metal SmBi using angle-resolved photoemission spectroscopy (ARPES). The experimental results exhibit multiple Fermi pockets around the $\bar{\Gamma}$ and \bar{M} points along with a band inversion in the spectrum along the $\bar{\Gamma}$ - \bar{M} line consistent with the density functional theory results. In addition, ARPES data reveal Dirac cones at the $\bar{\Gamma}$ and \bar{M} points within the energy gap of the bulk bands. The Dirac cone at \bar{M} exhibits a distinct Dirac point and is intense in the high-photon-energy data, while the Dirac cone at $\bar{\Gamma}$ is intense at low photon energies. Employing ultrahigh-resolution ARPES, we discover destruction of a Fermi surface constituted by the surface states across the Néel temperature of 9 K. Interestingly, the Dirac cone at $\bar{\Gamma}$ is found to be gapped at 15 K, and the behavior remains similar across the magnetic transition. These results reveal complex momentum-dependent gap formation and Fermi surface destruction across the magnetic transition in an exotic correlated topological material; the interplay between magnetism and topology in this system calls for ideas beyond the existing theoretical models.

DOI: [10.1103/PhysRevB.106.085132](https://doi.org/10.1103/PhysRevB.106.085132)

I. INTRODUCTION

Topological insulators (TIs) have attracted much attention due to their potential for quantum science and device applications [1]. In these materials, spin-orbit coupling (SOC) leads to band inversion, and topological surface states (TSSs) possessing Dirac-cone-like dispersion and vortexlike spin texture appear inside the inverted band gap in the presence of time-reversal and/or mirror symmetry [2]. In topological (Dirac and Weyl) semimetals, the valence and conduction bands touch at discrete points or extended lines within the bulk Brillouin zone (BBZ). In Dirac semimetals, the doubly degenerate bands respecting inversion and time-reversal symmetries cross at the Dirac point (DP). Breaking of time-reversal or inversion symmetry lifts the band degeneracy to realize Weyl semimetals [3,4]. Research in this field significantly involves the discovery of new materials where such physics can be realized. Recently, the *RSb-RBi* (*R* = rare earth) family of materials have been studied extensively reporting Dirac states and giant magnetoresistance [5–14]. For example, LaBi exhibits three Dirac cones: one at $\bar{\Gamma}$ and two at \bar{M} of the surface Brillouin zone (SBZ) [9]. The Dirac cone at $\bar{\Gamma}$ is gapped and exhibits asymmetric mass acquisition [10]. Another study [12] reported one Dirac cone at \bar{M} .

Electron correlation is expected to influence the effective mass of Dirac fermions leading to exotic properties. The Kondo insulator SmB₆ was proposed to be in this class and host TSSs within the Kondo gap [15]. Extensive studies re-

ported the interesting surface and bulk electronic structure of SmB₆ although its topological behavior is widely debated [16–20]. The properties of (Pr, Sm)Sb and (Pr, Sm)Bi were studied extensively to probe the origin of extreme magnetoresistance in these materials [21,22]. SmBi belongs to this class and is predicted to host TSSs from band structure calculations [23], whereas an angle-resolved photoemission spectroscopy (ARPES) study [7] does not show evidence of such TSSs. A recent study of the magnetic and transport properties of SmBi shows an antiferromagnetic (AFM) transition at 9 K, Kondo-type resistivity, and a signature of the nontrivial Berry phase [24]. Clearly, SmBi can be a candidate material for the study of interplay between topology and magnetism. Here, we studied the electronic structure of SmBi employing high-resolution ARPES and first-principles calculations and discover the coexistence of widely varying Dirac fermions and their unusual evolution across the magnetic transition.

II. EXPERIMENTAL AND COMPUTATIONAL DETAILS

High-quality single crystals of SmBi were grown by the flux method [24]. ARPES measurements were performed on the (001) surface prepared by cleaving at 6 K using an ultrahigh-resolution μ -laser ARPES setup ($h\nu = 6.3$ eV; R4000 analyzer) and *s*-polarization geometry at Hiroshima Synchrotron Radiation Center (HiSOR) (energy resolution < 260 μ eV, angular resolution $< 0.05^\circ$) [25]. The synchrotron-ARPES measurements were done at the BL-1 beamline, HiSOR [26] (energy resolution = 20 meV, angular resolution = 0.1°). The Fermi level ϵ_F was determined using a gold film evaporated onto the sample holder. Electronic

*Corresponding author: kbmaiti@tifr.res.in

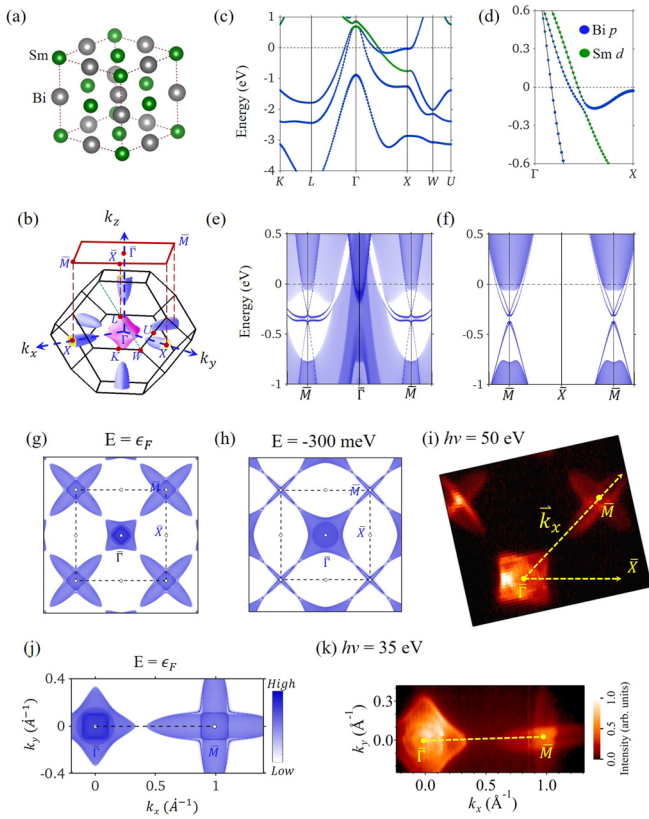


FIG. 1. (a) Crystal structure of SmBi. (b) Fermi surfaces within the BBZ and (001) surface projected SBZ. There is a spherical hole pocket (not shown) inside the star-shaped hole pockets at $\bar{\Gamma}$. (c) Band structure of nonmagnetic SmBi including SOC. The blue and green markers highlight Bi $6p$ and Sm $5d$ states. (d) Close-up of bands along the Γ - X line exhibiting bulk band inversion. (e) and (f) Calculated (001) surface band structure along \bar{M} - $\bar{\Gamma}$ - \bar{M} (e) and \bar{M} - \bar{X} - \bar{M} (f) of the SBZ. Two Dirac cones at the \bar{M} point are resolved. Dirac states at the $\bar{\Gamma}$ point are masked with bulk band projections. (g) and (h) Calculated surface band contours at the Fermi energy ($E = \epsilon_f$) (g) and $E = -300$ meV (near the Dirac point) (h). (i) Experimental Fermi surface collected with a photon energy of 50 eV. (j) Calculated and (k) measured surface Fermi contours along the $\bar{\Gamma}$ - \bar{M} direction.

structure calculations were performed using the projector augmented wave method as implemented in the Vienna *ab initio* simulation package (VASP) [27,28]. The generalized gradient approximation (GGA) was employed to include the exchange-correlation effects [29]. For magnetic solutions, on-site Coulomb interaction was added for Sm $4f$ electrons within the GGA+ U scheme [30]. An energy cutoff of 480 eV was used for the plane-wave basis set, and a $11 \times 11 \times 11$ k mesh was considered for BBZ integration. Topological properties were obtained by employing the materials-specific tight-binding Hamiltonian using the WANNIERTOOLS package [31,32].

III. RESULTS AND DISCUSSION

The crystal structure of SmBi (space group $Fm\bar{3}m$) and the calculated bulk Fermi surfaces (FSs) are shown in Figs. 1(a) and 1(b), respectively. In Fig. 1(b), the high-symmetry points

of the BBZ and their projection on the (001) surface are also shown. The calculated bulk band structure in Fig. 1(c) exhibits three bands crossing ϵ_F along the Γ - X line; the close-up of these bands [see Fig. 1(d)] illustrates a band inversion between Bi p and Sm d derived bands at the X points. Antiband crossing features are resolved along the Γ - X line indicating that valence and conduction bands are locally separated at each k point. The Z_2 topological invariant obtained by calculating inversion eigenvalues of the occupied bands at eight time-reversal-invariant momenta is 1 suggesting the presence of a nontrivial topological phase in this system [2,23]. Figures 1(e) and 1(f) show the calculated (001) surface band structure along the \bar{M} - $\bar{\Gamma}$ - \bar{M} and \bar{M} - \bar{X} - \bar{M} lines. Two Dirac cones are resolved at \bar{M} consistent with the projection of two X points with inverted bulk bands. An additional Dirac cone is expected at $\bar{\Gamma}$ although it is masked with the bulk projections. The calculated surface Fermi contours are shown in Fig. 1(g). They exhibit a star-shaped Fermi pocket near \bar{M} and a circular hole pocket around $\bar{\Gamma}$. The square-shaped pocket around $\bar{\Gamma}$ is the projection of electron pockets at X of the BBZ. Ellipsoidal pockets around \bar{M} are the projection of the electron pockets of the X points. The surface band contours close to the DP ($E = -300$ meV) in Fig. 1(h) unfold the surface bands.

Experimental FSs measured using 50 and 35 eV photon energies are shown in Figs. 1(i) and 1(k). We observe one circular-shaped FS inside a star-shaped FS at $\bar{\Gamma}$ representing the two-hole pockets consistent with the calculations. Overlapping elliptical Fermi pockets at \bar{M} are the projection of electron pockets. There is an additional intense circle inside the bulk circular hole pocket at $\bar{\Gamma}$ in the 35-eV data. The calculated and measured Fermi contours are in substantial agreement as shown in Figs. 1(j) and 1(k).

In Figs. 2(a) and 2(h), we show the energy bands measured along the $\bar{\Gamma}$ - \bar{M} line using varied photon energies. The calculated bulk band structure is shown by lines in Fig. 2(a) exhibiting a good description. The bands corresponding to two-hole pockets around $\bar{\Gamma}$ and an electron pocket at \bar{M} are evident in the figure. The outer hole band and electron band in Figs. 2(a) and 2(i) exhibit band inversion along the $\bar{\Gamma}$ - \bar{M} line due to Bi $6p$ -Sm $5d$ overlap consistent with the density functional theory (DFT) results.

Interestingly, 35-eV ARPES data show a Dirac cone around $\bar{\Gamma}$. Another Dirac cone at \bar{M} is observed at high photon energies. The dependence of the intensity of Dirac bands on the photon energy arises from the photoemission matrix element effects [33,34]. Clearly, the properties of the Dirac cones at $\bar{\Gamma}$ and \bar{M} are significantly different. Earlier studies of the same material class reported two Dirac cones at \bar{M} in some cases [7-9] and one Dirac cone in others [12,13]. We identify one cone in the 90-eV data shown in Fig. 2(j) and the corresponding momentum distribution curves (MDCs) in Fig. 2(k), which is similar to the latter case and/or the Dirac points in SmBi are too close to be detected distinctly. The DP (vertical dashed line) in the energy distribution curves (EDCs) at \bar{M} shown in Fig. 2(l) does not shift with the change in photon energy (Γ on the k_z axis appears at 51 and 85 eV assuming an inner potential of 14 eV). The absence of k_z dependence of the DP suggests two-dimensional behavior of Dirac fermions.

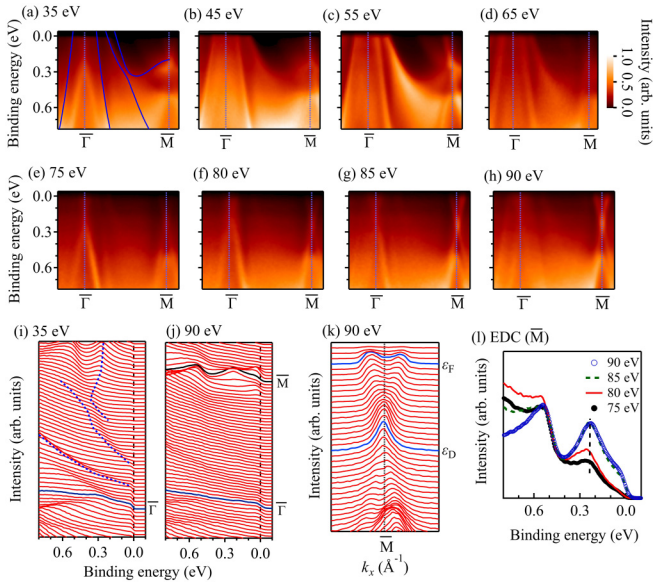


FIG. 2. (a)–(h) ARPES data along the $\bar{\Gamma}$ – \bar{M} line measured with photon energies 35–90 eV. The solid lines in (a) are the DFT results. (i) EDCs of the 35-eV ARPES data near $\bar{\Gamma}$ showing the band inversion and a distinct Dirac cone at $\bar{\Gamma}$. (j) EDCs and (k) MDCs of 90-eV ARPES data show a Dirac cone at \bar{M} . (l) EDCs at \bar{M} at different photon energies exhibiting a Dirac node (vertical dashed line) almost at the same energy.

The band structure along the $\bar{\Gamma}$ – \bar{X} line measured using 25 eV photon energy is shown in Fig. 3(a), and the corresponding MDCs are shown in Fig. 3(b). The ARPES data at 30–55 eV are shown in Figs. 3(c)–3(h). Similar to Fig. 2, we observed two distinct bands cross ϵ_F forming two hole pockets around $\bar{\Gamma}$. Intense bands beyond 1.5 eV are also observed. These results represent the bulk band structure and are in good agreement with the DFT results as shown by solid lines superimposed on the experimental data. The bands forming a Dirac cone at $\bar{\Gamma}$ in addition to the bulk bands are clearly visible in the 25–35 eV photon energy spectra. While the intensity of the upper cone part is weak, the lower part is intense at 25 eV and gradually becomes weaker with the increase in photon energy due to the matrix element effect [33].

In Fig. 4, we show the ultrahigh-resolution laser ARPES data. The data at 15 K exhibit three circular Fermi pockets as marked by the dashed lines. The outermost circle represents the bulk hole pocket as seen in the DFT results and the synchrotron data in Fig. 1. The signature of a surface Fermi pocket is also observed in the synchrotron-ARPES data [see Fig. 1(k)]; ultrahigh-resolution laser ARPES data resolved the distinct signature of two pockets due to the surface bands. Interestingly, the outer surface pocket is absent in the 6-K data suggesting destruction of the surface states derived Fermi pockets across the magnetic transition.

The bands along cuts 1 and 2 are shown in Figs. 4(c)–4(f). At 15 K, intense bands cross ϵ_F that form the innermost Fermi pocket. A Dirac cone is seen with the DP around 320 meV at $\bar{\Gamma}$. The lower part of the cone is much more intense compared with the upper part. Despite weaker intensity, distinct linear bands are observed to cross ϵ_F and form the middle Fermi

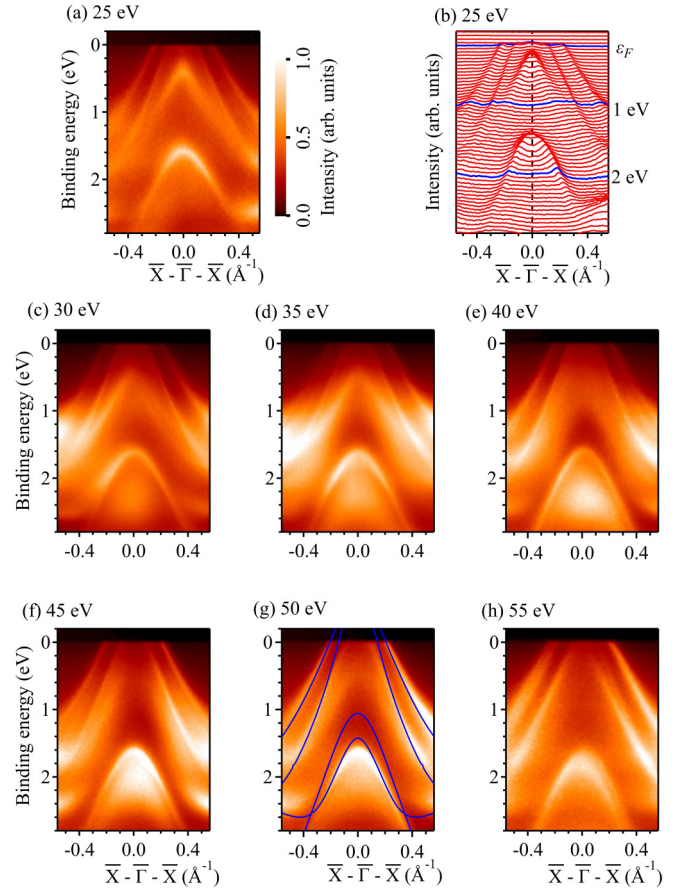


FIG. 3. (a) ARPES spectra measured at 30 K along the $\bar{\Gamma}$ – \bar{X} vector using 25 eV photon energy and (b) their corresponding MDCs. (c)–(h) ARPES spectra using similar conditions and photon energies varying from 30 to 55 eV. Solid lines in (g) are the DFT results.

pocket as evident in Figs. 4(c) and 4(e). This is verified by the MDCs at ϵ_F in Fig. 4(k); three distinct peaks in the 15-K data reflect the signature of three Fermi pockets. The middle peak around 0.093 \AA^{-1} is absent in the 6-K data as also observed in the FS plot in Fig. 4(b). The EDCs in Figs. 4(h) and 4(j) suggest that the linear Dirac bands form an energy gap below the Néel temperature. The EDCs at 15 K shown in Figs. 4(g) and 4(i) do not exhibit this property. To confirm the gap formation, we plot the EDCs at 15 and 6 K at k_F ($= 0.093 \text{ \AA}^{-1}$) in Fig. 4(l), which show significant intensity loss at ϵ_F at 6 K compared with the 15-K data. These results demonstrate the destruction of the Fermi pocket across the antiferromagnetic transition; a signature of the complex scenario of magnetism of the topological states.

We now analyze the spectral intensities at the DP in Fig. 4(m). The EDCs show a distinct signature of a two-peak structure as seen in the fit using Voigt functions for the 6-K data along cut 2 in Fig. 4(n). The energy gap is estimated to be about $25 (\pm 5) \text{ meV}$ at the DP. The results are quite similar for the data along cut 1 too. Interestingly, if we shift the 6-K data by 11 meV towards lower binding energy [see solid lines in Fig. 4(m)], they superimpose on the 15-K data well. This suggests that the properties of the Dirac fermions near the DP are not significantly influenced by the antiferromagnetic order.

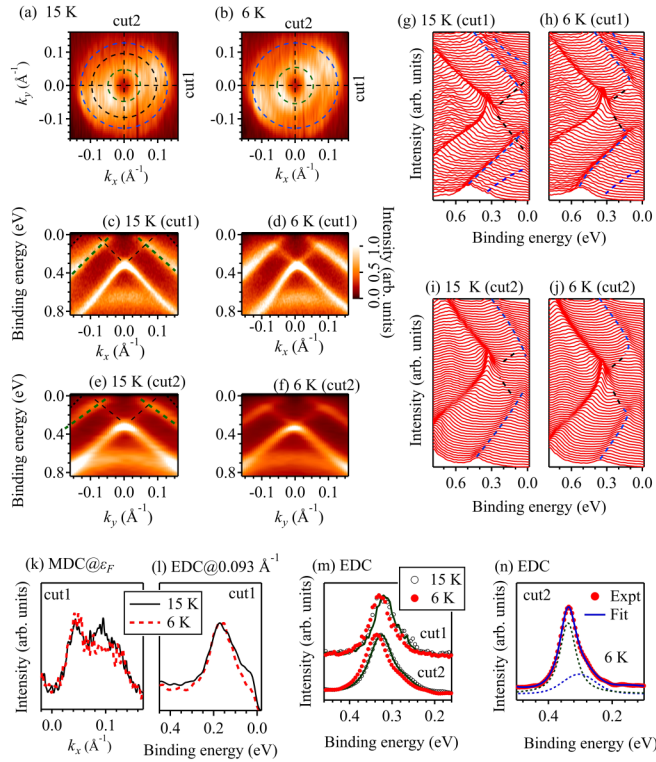


FIG. 4. Fermi surface at (a) 15 K and (b) 6 K in the ultrahigh-resolution laser ARPES data. Band dispersions along cut 1 at (c) 15 K and (d) 6 K and along cut 2 at (e) 15 K and (f) 6 K. Corresponding EDCs along cut 1 at (g) 15 K and (h) 6 K and along cut 2 at (i) 15 K and (j) 6 K; dashed lines are the hand-drawn curves. (k) MDCs at ϵ_F at 15 K (solid line) and 6 K (dashed line) for cut 1. (l) EDCs at k_F ($= 0.093 \text{ \AA}^{-1}$) at 15 K (solid line) and 6 K (dashed line). (m) EDCs at $\bar{\Gamma}$ at 15 K (open circles) and 6 K (solid circles). Lines overlaid on the 15-K data represent the 6-K data shifted by 11 meV. (n) Fit of the EDC at $\bar{\Gamma}$ along cut 2 at 6 K showing an energy gap at the Dirac point. Dotted lines are the component peaks.

To investigate the AFM state theoretically, we show calculated energy bands in Fig. 5. We find that the inverted energy gap at \bar{M} is gradually reduced with enhancement in effective electron correlation strength U_{eff} among Sm $4f$ electrons. However, the overall properties of the bulk bands in Figs. 5(a)–5(c) are similar to the nonmagnetic case. The FS contours for $U_{\text{eff}} = 4$ and 10 eV are shown in Figs. 5(d) and 5(g). In Figs. 5(e) and 5(f), and in Figs. 5(h) and 5(i), the Dirac states at \bar{M} form an energy dispersion similar to the nonmagnetic phase along with a gap at the DP due to time-reversal symmetry breaking at the surface. Interestingly, a large gap appears at the DP at $\bar{\Gamma}$ shown in Figs. 5(e) and 5(h), which was absent in the nonmagnetic phase. To compare the FS with the ultrahigh-resolution data in Fig. 4, we show the FS around $\bar{\Gamma}$ in Fig. 5(j); the square-shaped FS is the projection of electron pockets at the X point. There are three Fermi pockets around $\bar{\Gamma}$ in the nonmagnetic solution; the surface contributions are not clearly visible due to heavy bulk band projections. The AFM solutions show two circular pockets as observed in the experiment indicating destruction of one surface FS across the AFM order. These results suggest that the DP gap at $\bar{\Gamma}$ and the destruction of the FS observed in experiments

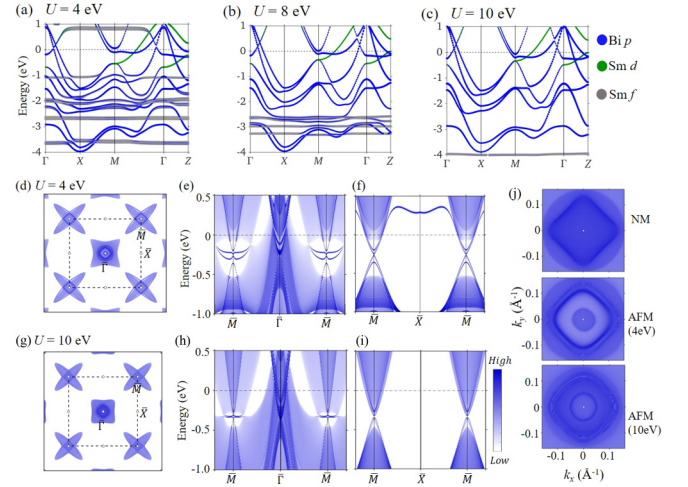


FIG. 5. Band structure of AFM SmBi in the conventional bulk Brillouin zone for (a) $U_{\text{eff}} = 4$ eV, (b) $U_{\text{eff}} = 8$ eV, and (c) $U_{\text{eff}} = 10$ eV. The Fermi level is adjusted to match the experimentally observed Dirac point at $\bar{\Gamma}$. (d) Calculated (001) surface projected Fermi contours. (e) and (f) E - k dispersions along the \bar{M} - $\bar{\Gamma}$ - \bar{M} (e) and \bar{M} - \bar{X} - \bar{M} (f) lines for $U_{\text{eff}} = 4$ eV. (g)–(i) Same as (d)–(f), but for $U_{\text{eff}} = 10$ eV. (j) Fermi surface around $\bar{\Gamma}$ for nonmagnetic (NM) and AFM solutions ($U_{\text{eff}} = 4, 10$ eV).

may be arising from antiferromagnetic interactions present in the system.

IV. CONCLUSIONS

In summary, we studied the electronic structure of the topological antiferromagnetic metal SmBi using high-resolution ARPES and density functional theory calculations. The energy bands along the $\bar{\Gamma}$ - \bar{M} line form a bulk band inversion between the Bi p and Sm d states. Intense surface bands forming a Dirac cone dispersion are resolved at the $\bar{\Gamma}$ and \bar{M} high-symmetry points. Ultrahigh-resolution laser ARPES data from the high-quality single crystals enabled the discovery of additional features in the electronic structure. The surface bands show the opening of an energy gap and Fermi surface destruction across the Néel temperature in accordance with our calculated results. The Dirac cone at the $\bar{\Gamma}$ point is gapped at 15 K, and the behavior remains similar across the magnetic transition. On the other hand, the Dirac cone at \bar{M} appears to be gapless. The interplay between topology and magnetism is an interesting and open area of research that is still in its infancy. The results for SmBi presented here reveal an exotic scenario of momentum-dependent gap formation at the Dirac point and destruction of one of the Fermi surfaces formed by topologically ordered surface states around $\bar{\Gamma}$ due to the long-range magnetic order which requires ideas beyond the existing theoretical models.

ACKNOWLEDGMENTS

The authors thank the Proposal Assessing Committee, HiSOR (Proposals No. 19BG053 and No. 20AU007); N-BARD Hiroshima University for liquid helium; and Yogendra

Kumar, School of Physical Sciences, University of Chinese Academy of Sciences, Beijing, for help. Financial support from Department of Atomic Energy (DAE), Government of India (Project No. RTI4003, DAE OM No.

1303/2/2019/R&D-II/DAE/2079 dated November 2, 2020), is thankfully acknowledged. K.M. thanks DAE-BRNS for financial support under the DAE-SRC-OI award program (21/08/2015-BRNS).

-
- [1] M. Z. Hasan and C. L. Kane, *Rev. Mod. Phys.* **82**, 3045 (2010).
- [2] L. Fu and C. L. Kane, *Phys. Rev. B* **76**, 045302 (2007); A. Maiti, R. P. Pandeya, B. Singh, K. K. Iyer, A. Thamizhavel, and K. Maiti, *ibid.* **104**, 195403 (2021); A. Maiti, A. Singh, K. K. Iyer, and A. Thamizhavel, *Appl. Phys. Lett.* **120**, 112102 (2022); Y. Tanaka, Zhi Ren, T. Sato, K. Nakayama, S. Souma, T. Takahashi, K. Segawa, and Y. Ando, *Nat. Phys.* **8**, 800 (2012).
- [3] S.-Y. Xu, C. Liu, S. K. Kushwaha, R. Sankar, J. W. Krizan, I. Belopolski, M. Neupane, G. Bian, N. Alidoust, T.-R. Chang, H.-T. Jeng, C.-Y. Huang, W.-F. Tsai, H. Lin, P. P. Shibayev, F.-C. Chou, R. J. Cava, and M. Z. Hasan, *Science* **347**, 294 (2015).
- [4] X. Wan, A. M. Turner, A. Vishwanath, and S. Y. Savrasov, *Phys. Rev. B* **83**, 205101 (2011).
- [5] M. Zeng, C. Fang, G. Chang, Y.-A. Chen, T. Hsieh, A. Bansil, H. Lin, and L. Fu, [arXiv:1504.03492](https://arxiv.org/abs/1504.03492); F. F. Tafti, Q. D. Gibson, S. K. Kushwaha, N. Haldolaarachdhige, and R. J. Cava, *Nat. Phys.* **12**, 272 (2015); F. F. Tafti, Q. Gibson, S. Kushwaha, J. W. Krizan, N. Haldolaarachdhige, and R. J. Cava, *Proc. Natl. Acad. Sci. USA* **113**, E3475 (2016); J. He, C. Zhang, N. J. Ghimire, T. Liang, C. Jia, J. Jiang, S. Tang, S. Chen, Y. He, S.-K. Mo, C. C. Hwang, M. Hashimoto, D. H. Lu, B. Moritz, T. P. Devereaux, Y. L. Chen, J. F. Mitchell, and Z.-X. Shen, *Phys. Rev. Lett.* **117**, 267201 (2016); M. Neupane, M. M. Hosen, I. Belopolski, N. Wakeham, K. Dimitri, N. Dhakal, J.-X. Zhu, M. Z. Hasan, E. D. Bauer, and F. Ronning, *J. Phys.: Condens. Matter* **28**, 23LT02 (2016); N. Alidoust, A. Alexandradinata, S.-Y. Xu, I. Belopolski, S. K. Kushwaha, M. Zeng, M. Neupane, G. Bian, C. Liu, D. S. Sanchez, P. P. Shibayev, H. Zheng, L. Fu, A. Bansil, H. Lin, R. J. Cava, and M. Z. Hasan, [arXiv:1604.08571v1](https://arxiv.org/abs/1604.08571v1); H.-Y. Yang, T. Nummy, H. Li, S. Jaszewski, M. Abramchuk, D. S. Dessau, and F. F. Tafti, *Phys. Rev. B* **96**, 235128 (2017); **97**, 079903(E) (2018).
- [6] A. Svane, V. Kanchana, G. Vaitheeswaran, G. Santi, W. M. Temmerman, Z. Szotek, P. Strange, and L. Petit, *Phys. Rev. B* **71**, 045119 (2005).
- [7] P. Li, Z. Wu, F. Wu, C. Cao, C. Guo, Y. Wu, Y. Liu, Z. Sun, C.-M. Cheng, D.-S. Lin, F. Steglich, H. Yuan, T.-C. Chiang, and Y. Liu, *Phys. Rev. B* **98**, 085103 (2018).
- [8] X. H. Niu, D. F. Xu, Y. H. Bai, Q. Song, X. P. Shen, B. P. Xie, Z. Sun, Y. B. Huang, D. C. Peets, and D. L. Feng, *Phys. Rev. B* **94**, 165163 (2016).
- [9] J. Nayak, S.-C. Wu, N. Kumar, C. Shekhar, S. Singh, J. Fink, E. E. D. Rienks, G. H. Fecher, S. S. P. Parkin, B. Yan, and C. Felser, *Nat. Commun.* **8**, 13942 (2017).
- [10] Y. Wu, T. Kong, L.-L. Wang, D. D. Johnson, D. Mou, L. Huang, B. Schruck, S. L. Bud'ko, P. C. Canfield, and A. Kaminski, *Phys. Rev. B* **94**, 081108(R) (2016).
- [11] C. Guo, C. Cao, M. Smidman, F. Wu, Y. Zhang, F. Steglich, F.-C. Zhang, and H. Yuan, *npj Quantum Mater.* **2**, 39 (2017); Q.-H. Yu, Y.-Y. Wang, R. Lou, P.-J. Guo, S. Xu, K. Liu, S. Wang, and T.-L. Xia, *Europhys. Lett.* **119**, 17002 (2017); O. Pavlosiuk, P. Swatek, D. Kaczorowski, and P. Wiśniewski, *Phys. Rev. B* **97**, 235132 (2018); D. D. Liang, Y. J. Wang, C. Y. Xi, W. L. Zhen, J. Yang, L. Pi, W. K. Zhu, and C. J. Zhang, *APL Mater.* **6**, 086105 (2018); H.-Y. Yang, J. Gaudet, A. A. Aczel, D. E. Graf, P. Blaha, B. D. Gaulin, and F. Tafti, *Phys. Rev. B* **98**, 045136 (2018); T. J. Nummy, J. A. Waugh, S. P. Parham, Q. Liu, H.-Y. Yang, H. Li, X. Zhou, N. C. Plumb, F. F. Tafti, and D. S. Dessau, *npj Quantum Mater.* **3**, 24 (2018).
- [12] R. Lou, B.-B. Fu, Q. N. Xu, P.-J. Guo, L.-Y. Kong, L.-K. Zeng, J.-Z. Ma, P. Richard, C. Fang, Y.-B. Huang, S.-S. Sun, Q. Wang, L. Wang, Y.-G. Shi, H. C. Lei, K. Liu, H. M. Weng, T. Qian, H. Ding, and S.-C. Wang, *Phys. Rev. B* **95**, 115140 (2017).
- [13] B. Feng, J. Cao, M. Yang, Y. Feng, S. Wu, B. Fu, M. Arita, K. Miyamoto, S. He, K. Shimada, Y. Shi, T. Okuda, and Y. Yao, *Phys. Rev. B* **97**, 155153 (2018).
- [14] M. M. Hosen, G. Dhakal, B. Wang, N. Poudel, B. Singh, K. Dimitri, F. Kabir, C. Sims, S. Regmi, W. Neff, A. B. Sarkar, A. Agarwal, D. Murray, F. Weickert, K. Gofryk, O. Pavlosiuk, P. Wiśniewski, D. Kaczorowski, A. Bansil, and M. Neupane, *Sci. Rep.* **10**, 12961 (2020); K. Kuroda, M. Ochi, H. S. Suzuki, M. Hirayama, M. Nakayama, R. Noguchi, C. Bareille, S. Akebi, S. Kunisada, T. Muro, M. D. Watson, H. Kitazawa, Y. Haga, T. K. Kim, M. Hoesch, S. Shin, R. Arita, and T. Kondo, *Phys. Rev. Lett.* **120**, 086402 (2018).
- [15] M. Dzero, K. Sun, V. Galitski, and P. Coleman, *Phys. Rev. Lett.* **104**, 106408 (2010).
- [16] M. Neupane, N. Alidoust, S.-Y. Xu, T. Kondo, Y. Ishida, D. J. Kim, Chang Liu, I. Belopolski, Y. J. Jo, T.-R. Chang, H.-T. Jeng, T. Durakiewicz, L. Balicas, H. Lin, A. Bansil, S. Shin, and Z. Fisk, and M. Z. Hasan, *Nat. Commun.* **4**, 2991 (2013).
- [17] J. Jiang, S. Li, T. Zhang, Z. Sun, F. Chen, Z. R. Ye, M. Xu, Q. Q. Ge, S. Y. Tan, X. H. Niu, M. Xia, B. P. Xie, Y. F. Li, X. H. Chen, H. H. Wen, and D. L. Feng, *Nat. Commun.* **4**, 3010 (2013).
- [18] N. Xu, X. Shi, P. K. Biswas, C. E. Matt, R. S. Dhaka, Y. Huang, N. C. Plumb, M. Radovic, J. H. Dil, E. Pomjakushina, K. Conder, A. Amato, Z. Salman, D. M. Paul, J. Mesot, H. Ding, and M. Shi, *Phys. Rev. B* **88**, 121102(R) (2013).
- [19] J. D. Denlinger, J. W. Allen, J.-S. Kang, K. Sun, J.-W. Kim, J. H. Shim, B. I. Min, D.-J. Kim, and Z. Fisk, [arXiv:1312.6637](https://arxiv.org/abs/1312.6637).
- [20] A. P. Sakhya and K. Maiti, *Sci. Rep.* **10**, 1262 (2020).
- [21] Z. Wu, F. Wu, P. Li, C. Guo, Y. Liu, Z. Sun, C.-M. Cheng, T.-C. Chiang, C. Cao, H. Yuan, and Y. Liu, *Phys. Rev. B* **99**, 035158 (2019).
- [22] A. Vashist, R. K. Gopal, D. Srivastava, M. Karppinen, and Y. Singh, *Phys. Rev. B* **99**, 245131 (2019).
- [23] X. Duan, F. Wu, J. Chen, P. Zhang, Y. Liu, H. Yuan, and C. Cao, *Commun. Phys.* **1**, 71 (2018).

- [24] A. P. Sakhya, P. L. Paulose, A. Thamizhavel, and K. Maiti, *Phys. Rev. Materials* **5**, 054201 (2021).
- [25] H. Iwasawa, E. F. Schwier, M. Arita, A. Ino, H. Namatame, M. Taniguchi, Y. Aiura, and K. Shimada, *Ultramicroscopy* **182**, 85 (2017).
- [26] H. Iwasawa, K. Shimada, E. F. Schwier, M. Zheng, Y. Kojima, H. Hayashi, J. Jiang, M. Higashiguchi, Y. Aiura, H. Namatame, and M. Taniguchi, *J. Synchrotron Radiat.* **24**, 836 (2017).
- [27] W. Kohn and L. J. Sham, *Phys. Rev.* **140**, A1133 (1965).
- [28] G. Kresse and D. Joubert, *Phys. Rev. B* **59**, 1758 (1999).
- [29] J. P. Perdew, K. Burke, and M. Ernzerhof, *Phys. Rev. Lett.* **77**, 3865 (1996).
- [30] S. L. Dudarev, G. A. Botton, S. Y. Savrasov, C. J. Humphreys, and A. P. Sutton, *Phys. Rev. B* **57**, 1505 (1998).
- [31] N. Marzari and D. Vanderbilt, *Phys. Rev. B* **56**, 12847 (1997).
- [32] Q. Wu, S. Zhang, H.-F. Song, M. Troyer, and A. A. Soluyanov, *Comput. Phys. Commun.* **224**, 405 (2018).
- [33] J. J. Yeh and I. Lindau, *At. Data Nucl. Data Tables* **32**, 1 (1985).
- [34] A. A. Kordyuk, T. K. Kim, V. B. Zabolotnyy, D. V. Evtushinsky, M. Bauch, C. Hess, B. Büchner, H. Berger, and S. V. Borisenko, *Phys. Rev. B* **83**, 081303(R) (2011).